

Evidence for multi-charge flux quantization in kagome superconductor ring devices

Jun Ge^{1†}, Pinyuan Wang^{1†}, Ying Xing^{1,2}, Qiangwei Yin³, Anqi Wang^{4,5}, Jie Shen^{4,6},
Hechang Lei³, Ziqiang Wang⁷ & Jian Wang^{1,8,9*}

¹International Center for Quantum Materials, School of Physics, Peking University, Beijing 100871, China.

²State Key Laboratory of Heavy Oil Processing, College of New Energy and Materials, China University of Petroleum, Beijing 102249, China.

³Beijing Key Laboratory of Optoelectronic Functional Materials & Micro-Nano Devices, Department of Physics, Renmin University of China, Beijing 100872, China.

⁴Beijing National Laboratory for Condensed Matter Physics, Institute of Physics, Chinese Academy of Sciences, Beijing 100190, China.

⁵School of Physical Sciences, University of Chinese Academy of Sciences, Beijing 100049, China.

⁶Songshan Lake Materials Laboratory, Dongguan 523808, China.

⁷Department of Physics, Boston College, Chestnut Hill, MA 0246, USA.

⁸Collaborative Innovation Center of Quantum Matter, Beijing 100871, China.

⁹Hefei National Laboratory, Hefei 230088, China.

*Corresponding author. Email: jianwangphysics@pku.edu.cn (J.W.).

† These authors contribute equally.

The flux quantization is a key indication of electron pairing in superconductors. For example, the well-known $h/2e$ flux quantization is considered strong evidence for the existence of the charge- $2e$, two-electron Cooper pairs. Here we report evidence for multi-charge flux quantization in mesoscopic ring devices fabricated using the transition-metal kagome superconductor CsV_3Sb_5 . We perform systematic magneto-transport measurements and observe unprecedented quantization of magnetic flux in units of $h/4e$ and $h/6e$ in magnetoresistance oscillations. Specifically, at low temperatures, magnetoresistance oscillations with period $h/2e$ are detected, as expected from the flux quantization for charge- $2e$ superconductivity. We find that the $h/2e$ oscillations are suppressed and replaced by resistance oscillations with $h/4e$ periodicity when temperature is increased. Increasing the

temperature further suppresses the $h/4e$ oscillations and robust resistance oscillations with $h/6e$ periodicity emerge as evidence for charge- $6e$ flux quantization. Our observations provide the first experimental evidence for the existence of multi-charge flux quanta and emergent quantum matter exhibiting higher-charge superconductivity in the strongly fluctuating region above the charge- $2e$ Cooper pair condensate, revealing new insights into the intertwined and vestigial electronic order in kagome superconductors.

Superconductivity was discovered more than one century ago and described by the Bardeen–Cooper–Schrieffer (BCS) theory in terms of the condensation of charge- $2e$ Cooper pairs (1, 2). Flux quantization in units of the charge- $2e$ flux quantum $h/2e$, where h is the Planck constant and e is the elementary charge, is a key signature of the electron pairing in BCS superconductors. The observations of the $h/2e$ flux quantization served as key experimental evidence of the BCS theory of conventional superconductors (SCs) (3–5). Superconductivity via the condensation of higher charges, such as bound states of electron quartets or sextets (i.e. charge- $4e$ or charge- $6e$), has been proposed theoretically under various conditions where the conventional charge- $2e$ superconductivity is suppressed (6–15). Despite intensive theoretical studies, whether higher-charge superconductivity exists and the many of its basic properties remain mysterious and illusive due to the lack of experimental evidence. For charge- Q superconductivity with $Q=2ne$ arise, there must exist experimental evidence for flux quantization in units of the charge- Q flux quantum $\Phi_0=h/2ne$.

Here, we report the observation of flux quantization in units of Φ_0^{4e} ($h/4e$) and Φ_0^{6e} ($h/6e$) in ring devices of the newly emerged kagome superconductor CsV_3Sb_5 . We fabricate superconducting CsV_3Sb_5 ring devices with various sizes and perform systematic magneto-transport measurements. At low temperatures, magnetoresistance oscillations with period of the charge- $2e$ flux quantum $h/2e$ are detected, as expected from the flux quantization for charge- $2e$ superconductivity. The $h/2e$ oscillations are suppressed and replaced by resistance oscillations with $h/4e$ periodicity as the temperature is increased. When the temperature is further increased toward the onset of the superconductivity, the $h/4e$ oscillations vanish and novel resistance oscillations with a period equaling to $1/3$ of the period of $h/2e$ oscillations emerge. Careful measurements and analysis on many ring devices indicate consistently that these resistance oscillations with the period equaling to $1/2$ and $1/3$ of the $h/2e$ oscillations reveal the existence of flux quantization in units of charge- $4e$ and charge- $6e$ (flux quanta Φ_0^{4e} and Φ_0^{6e}), respectively. Our observations provide the first and direct experimental evidence of flux quantization in units of the multi-charge flux quanta in kagome superconductor ring devices and points to the possible existence of unprecedented higher-charge superconducting quantum states in the strongly fluctuating region of kagome superconductors.

Results

Bulk CsV_3Sb_5 crystallizes into the $P6/mmm$ space group (Fig. 1A), with a two-dimensional (2D) kagome network of vanadium (V) cations coordinated by octahedra of antimony (Sb) (16, 17). Adjacent kagome sheets are separated by

layers of cesium (Cs) ions (16, 17). Bulk CsV₃Sb₅ undergoes charge density wave transition at around ~ 94 K before developing superconductivity (17) at about 2.5 K. Due to the combined effects of geometric frustration, quantum interference and electron correlation, and electron-lattice interaction on the kagome network, a diverse set of correlated and topological electronic states has been discovered, including superconductivity and pair density wave order (12, 18-31). In this work, we fabricate the CsV₃Sb₅ ring structures by etching the kagome superconductor thin flakes exfoliated from bulk samples as shown in the schematic Fig. 1B. Figure 2A displays the temperature dependence of the resistance of CsV₃Sb₅ ring device s1 with a thickness of ~ 14.6 nm in zero magnetic field, with the false-colored scanning electron microscope (SEM) image shown in the inset and the atomic force microscopy results in Fig. S1. The superconducting transition with the onset temperature $T_c^{onset} \sim 3.9$ K and the zero resistance temperature $T_c^{zero} \sim 1.1$ K marked in the figure delineate an extended superconducting fluctuation region where new quantum states of paired matter may arise.

We then carry out systematic magneto-transport measurements on the CsV₃Sb₅ ring devices. The measured resistance (R)-magnetic field (H) curves shown in Fig. S2A exhibit oscillations at temperatures from 0.1 K to 1.0 K. By subtracting the smoothly rising (in H) resistance backgrounds in the R - H curves, the oscillations become more pronounced as shown in Fig. 2B at various temperatures, where dashed and solid lines guide the dips and peaks, respectively. We index the dips and peaks of the oscillations by an integer or half-integer n and the corresponding magnetic field by H_n . The positions of the dashed or solid line associated with an index n is chosen to make sure that most of the corresponding dips and peaks on different curves can be properly located. Plotting H_n versus n reveals a clear linear dependence (Fig. 2H), indicating that these oscillations are periodic in H , as expected from the quantization of the magnetic field flux through the ring $\Phi = n\Phi_0$, where n is an integer, in unit of the charge- $2e$ superconducting flux quantum Φ_0 . Using the measured period of the oscillations in Fig. 2B, i.e. $\Delta H_{2e} \sim 750$ Oe, and setting $\Phi_0 = h/2e = S \cdot \Delta H_{2e}$, we obtain the effective ring area $S \approx 0.0276 \mu\text{m}^2$, which is marked by the red rectangle in the inset of Fig. 2A. Note that if the effective area were larger, the condition for flux quantization would imply Cooper pairs of fractional charged quasiparticles, which is unlikely for this system. We thus consider the oscillations with period of ~ 750 Oe as the charge- $2e$ ($h/2e$) oscillations with the effective area close to inner hole area. We will return to the physical implications in the discussion section.

Surprisingly, upon increasing the temperature to 1.65 K and above into the broad superconducting transition region, new oscillations are observed (Fig. 2C)

with a different period in magnetic field $\Delta H \sim 350$ Oe as confirmed by the linear relation between n and H_n (Fig. 2H). These emergent oscillations corresponds to a magnetic flux through the ring $\Phi = S \cdot \Delta H = 0.97 \times 10^{-15}$ Wb, using the same effective area $S \approx 0.0276 \mu\text{m}^2$ identified above and marked in the inset of Fig. 2A. Intriguingly, this value of the flux is very close to one-half of the charge- $2e$ flux quantum, i.e. the charge- $4e$ flux quantum $\Phi_0^{4e} = h/4e = 1.03 \times 10^{-15}$ Wb.

More strikingly, we find that the oscillations with period of ~ 350 Oe vanish when the temperature is further increased. Above 2.3 K, brand new oscillations in magnetic field emerge with the period $\Delta H \sim 250$ Oe (Figs. 2D-G). This value is remarkably 1/3 of that in the charge- $2e$ oscillations (~ 750 Oe) observed at low temperatures and corresponds to resistance oscillations due to flux quantization in units of an emergent charge- $6e$ flux quantum $\Phi_0^{6e} = h/6e = 0.69 \times 10^{-15}$ Wb, under the same effective area ($S \approx 0.0276 \mu\text{m}^2$). Indeed, the charge- $6e$ resistance oscillations in Figs. 2D-G are strong and robust over a wide field range (Fig. S4), exhibiting magnetic flux quantization $\Phi = n\Phi_0^{6e}$ down to zero magnetic field with a resistance minimum at $n=0$ (Figs. 2D, E). In Fig. 2I and Fig. S11A, the temperature evolution of the fast Fourier transform (FFT) of the resistance oscillations is presented in a waterfall plot. The positions of the FFT peaks show that the periodicity of the flux quantization in unit of the magnetic flux quantum changes from $\Phi_0 = h/2e$ at low temperatures to $\Phi_0^{4e} = h/4e$ at higher temperatures, and then to $\Phi_0^{6e} = h/6e$ at still higher temperatures on approaching the onset of the superconducting transition. Similar results have also been observed consistently in other CsV_3Sb_5 ring devices of similar dimensions. The results obtained on another device are summarized in Fig. S5.

It is important to note that these set of thick-rimmed ring devices leave room for the possibility that the oscillations with period of ~ 350 Oe and ~ 250 Oe were also $h/2e$ oscillations, but with larger effective areas. In the following, we will show that this possibility can be excluded and the effective area remains a constant for $h/2e$, $h/4e$ and $h/6e$ oscillations in a given CsV_3Sb_5 ring device. First, as shown in Fig. 2I and Fig. S11A, the FFT peak positions for $h/2e$, $h/4e$, and $h/6e$ oscillations respectively do not change with the temperature, indicating that the corresponding effective area maintains a constant with increasing temperatures. Second, there are no intermediate periodicities between the $h/2e$ ($h/4e$) and $h/4e$ ($h/6e$) oscillations, which further demonstrates the constant effective area for the observed oscillations. Moreover, the reliability of the constant effective area can be further verified by a new type of quantum oscillations observed together with the $h/6e$ oscillations in device s1 (Fig. S6). This new type of oscillation shows a large period ~ 1500 Oe and can persist down to zero magnetic field. Considering the

same effective area ($S \approx 0.0276 \mu\text{m}^2$) as the $h/2e$, $h/4e$, and $h/6e$ oscillations, the new type of oscillations (period ~ 1500 Oe) yields a periodicity with h/e flux quantization. If the effective area for this new type of oscillations is larger ($>0.0276 \mu\text{m}^2$), the charge must be fractional, which is very unlikely to emerge in vanadium-based kagome superconductors such as CsV_3Sb_5 . We have therefore demonstrated that the constant effective area ($S \approx 0.0276 \mu\text{m}^2$) defines all of the observed quantum oscillations and the proper identification of the $h/2e$, $h/4e$ and $h/6e$ flux quantization in the CsV_3Sb_5 ring device s1.

To further scrutinize the evidence for the extraordinary charge- $6e$ flux quantization and directly exclude the possibility of assigning the $h/6e$ oscillations as those of $h/2e$ under a different effective area, we fabricated micron-sized CsV_3Sb_5 ring devices with much larger hole area and ratio of hole size to wall width. The experimental data on device s2 with a hole area $\sim 0.96 \mu\text{m}^2$ are presented in Fig. 3. At low temperatures, resistance oscillations with period ~ 13.6 Oe in magnetic field are observed. Using the measured period of the oscillations in Fig. 3B, i.e. $\Delta H_{2e} \sim 13.6$ Oe, and setting $\Phi_0 = h/2e = S \cdot \Delta H_{2e}$, we obtain the effective area $S \approx 1.52 \mu\text{m}^2$, which is marked by the red rectangle in the inset of Fig. 3A. If a larger effective area, e.g. with boundaries in the middle of the rim ($S_{\text{middle}} \sim 2.01 \mu\text{m}^2$) were considered as the effective area, then the flux $\Phi = S_{\text{middle}} \cdot \Delta H = 2.734 \times 10^{-15} \text{ Wb} \approx h/0.77e$, would lead to fractional charges, which is unlikely in this system. Therefore, the oscillations at low temperatures in the large ring device s2 are $h/2e$ oscillations.

When the temperature is increased to 2.5 K and above, novel emergent oscillations are again observed (Fig. 3E), as in the smaller, thick-rimmed devices. The periodicity of these new oscillations is confirmed by the linear relation between n and H_n (Fig. 3F), which reveals a new period in magnetic field $\Delta H \sim 4.6$ Oe, equaling to $1/3$ of the period of the $h/2e$ oscillations (~ 13.6 Oe) observed at low temperatures. These small-period oscillations (~ 4.6 Oe) cannot be mistaken for $h/2e$ oscillations with a larger effective area in the micron-sized device s2, because if they were, the corresponding effective area (green rectangle in the inset of Fig. 3A) would be much larger than even the outer area of the ring device, which is physically impossible. Therefore, the oscillations with period of ~ 4.6 Oe are unambiguous evidence for flux quantization in unit of novel higher-charge magnetic flux quantum. Considering the extremities of device s2, i.e. an outer area $S_{\text{outer}} \sim 2.97 \mu\text{m}^2$ and an inner area $S_{\text{inner}} \sim 0.96 \mu\text{m}^2$, the oscillations period ~ 4.6 Oe imply that the flux quantum must satisfy: $\Phi_{\text{inner}} \leq \Phi \leq \Phi_{\text{outer}}$, where $\Phi_{\text{inner}} = S_{\text{inner}} \cdot \Delta H = 0.44 \times 10^{-15} \text{ Wb} \approx h/9e$ and $\Phi_{\text{outer}} = S_{\text{outer}} \cdot \Delta H = 1.366 \times 10^{-15} \text{ Wb} \approx h/3e$. This

means that the oscillations with period of ~ 4.6 Oe do not correspond to the $2e$ but the multi-charge of the flux quantum in the range of $3e$ to $9e$.

The evidence for a temperature-independent effective area discussed above encourages the use of the same effective area ($S \approx 1.52 \mu\text{m}^2$) determined for the low-temperature charge- $2e$ oscillations with period ~ 13.6 Oe and the oscillations with period ~ 4.6 Oe at higher temperatures, which corresponds to a magnetic flux through the ring $\Phi = S \cdot \Delta H = 0.699 \times 10^{-15}$ Wb. This value is remarkably close to the periodicity in unit of the charge- $6e$ superconducting flux quantum $\Phi_0^{6e} = h/6e = 0.69 \times 10^{-15}$ Wb. Similar results have also been obtained in two additional large ring devices s4 (Fig. S7) and s5 (Fig. S8). These results on devices with much larger hole areas provide arresting evidence for the discovery of robust $h/6e$ oscillations in CsV_3Sb_5 ring devices. In Fig. 4, we present the temperature evolution of the magnetoresistance oscillations as color intensity plots in unit of the magnetic flux Φ/Φ_0 over the broad superconducting transition region in the CsV_3Sb_5 ring devices. With the increase of the melting temperature, the periodicity of the oscillations changes from $h/2e$ to $h/4e$ and then to $h/6e$ in small thick-rimmed ring devices represented by s1, and from $h/2e$ to $h/6e$ in micron sized ring devices represented by s2, recapitulating our finding of multi-charge flux quantization in unit of charge- $4e$ and charge- $6e$ superconducting flux quanta.

Discussion

We stress that these extraordinary flux quanta originate from the extraordinary superconducting fluctuation region in CsV_3Sb_5 ring devices that is very broad with internal structures as reflected by the R - T curve. The physics in this fluctuation region is different and beyond what happens in the very sharp transition region of typical BCS superconductors. In the latter case, quantum oscillations experiments of the type we conducted are known as the Little-Parks oscillations (32) and are expected to produce only charge- $2e$ flux quantization. To further substantiate this fundamental difference and develop new insights, we studied ring devices made of conventional superconductor Nb (Fig. S9, S10) using identical fabrication methods. Two Nb ring devices are fabricated using the same FIB etching technique, under the same ion beam current, and protected by the PMMA layer of the same thickness. The measured R - T curve reveals a sharp superconducting transition in the Nb ring device n1 (onset temperature ~ 7.6 K and zero resistance temperature ~ 7.0 K, Fig. S9A) and n2 (onset temperature ~ 7.6 K and zero resistance temperature ~ 7.2 K, Fig. S10A). Indeed magnetoresistance measurements show only $h/2e$ oscillations in Nb ring devices in a narrow temperature regime (Fig. S9C, Fig. S10D) above the zero-resistance transition. The corresponding effective area

has a radius lying in the middle of the wall (inset of Fig. S9A for device n1 and Fig. S10A for device n2), which is in accord with the theoretical predictions for the Little-Parks oscillations in conventional superconductor ring devices (33). These experiments reassure that our device fabrication, measurements, and analysis have been tested to reproduce the expected physics in ordinary BCS superconductors, and further demonstrate that the remarkable observation of the multi-charge flux quantization is due to the never before encountered higher-charge superconducting quantum states in extended fluctuation region of CsV_3Sb_5 ring devices.

Another intriguing property, distinct from ordinary superconductors having sharp superconducting transitions, is that the observed resistance oscillations with different flux quantization in the strongly fluctuating superconductivity region all have the same effective area close to the inner hole area in the CsV_3Sb_5 ring devices (inset of Figs. 2A, 3A). In a recent insightful paper, Han and Lee (34) provided a possible theoretical explanation for our experimental observation. They studied the effective area for transporting charge- $4e$ and charge- $6e$ bound states across our thick-rimmed geometry devices (CsV_3Sb_5 ring device s1, s3) using the space-time formulation of time-dependent Ginzburg-Landau theory. Because the superconductivity is strongly fluctuating in the broad transition regime in the CsV_3Sb_5 ring devices, the optimal path is found to stick to the edge of the inner hole in order to reduce the fluctuations by proximity to the open area of the hole, leading to the effective area close to the inner area for $h/4e$ and $h/6e$ flux quantization. The result also applies to the strongly fluctuating charge- $2e$ state (34). The combined experimental and theoretical findings land convincing support for the observation of resistance oscillations with $h/4e$ and $h/6e$ flux quantization.

We now turn to the possible origin of the observed charge- $4e$ and charge- $6e$ flux quantization. There are theoretical proposals for fractional flux quantum in spin-triplet $p + ip$ superconductors (35, 36), and in vortices trapped at domain walls and twin boundaries in time-reversal symmetry breaking superconductors (37). However, these do not describe our observation because the fractional flux quantization under these settings only leads to nontrivial phase shift in the quantum oscillations, while the periodicity of the oscillations would remain at Φ_0 as the pairing is still charge- $2e$ in nature. More theoretical discussions are available in Supplementary Materials. While we cannot rule out the possibility where a fractional flux quantum results from a multicomponent superconductor where the phases of different charge- $2e$ condensates wind differently in the magnetic field (38), the observed sequential changes in the flux quantization under thermal melting are unnatural to be accounted for in this scenario.

The distinct charge- $4e$ and charge- $6e$ flux quanta observed in the flux quantization with increasing temperatures naturally suggests a sequential destruction of the phase coherent charge- $2e$ superconductivity and the emergence of phase coherent bound states of 4-electrons (or two Cooper pairs) and 6-electrons (or three Cooper pairs) in the strongly fluctuating transition region of the ring structures. This scenario is consistent with the theoretical proposal of the putative charge- $4e$ and charge- $6e$ superconductivity as vestigial ordered states following the melting of a novel charge- $2e$ superconducting state that simultaneously breaks crystalline symmetry, and is supported by the evidence for PDW order observed by STM in the kagome superconductor CsV_3Sb_5 (22). It was proposed theoretically that the staged melting of the hexagonal roton PDW can give rise to an orientation ordered charge- $4e$ hexatic superconductor with a $d+id$ symmetry by proliferating dislocations, followed by an isotropic s-wave charge- $6e$ superconductor by unbinding disclinations at higher temperatures (12). The sharp FFT peaks located at $6e/h$ for $h/6e$ oscillations in Fig. 2I with the nearly perfect periodicity down to zero magnetic field is indeed consistent with the most robust s-wave charge- $6e$ state in the isotropic phase proposed in this scenario. The chiral phase in the vestigial hexatic charge- $4e$ state, on the other hand, couples strongly to the strain fields, supercurrent fluctuations, and disclination defects (12), which limit the correlation length and hinders the ability of the charge- $4e$ bound states to move through the ring structure phase coherently. As a result, in contrast to the robust isotropic charge- $6e$ state, the charge- $4e$ state is more fragile, which is consistent with our observation that the $h/4e$ oscillations are relatively weak in small ring devices and difficult to discern in the micron-sized ring devices with much larger hole areas. Although the hexagonal PDW offers a physically intuitive picture for our observations, the origin of the observed charge- $6e$ flux quantization is wide open for future investigations, as is the mechanism for superconductivity and PDW order in the kagome superconductors.

In summary, we discovered quantum oscillations with the periodicity of multi-charge flux quantization in mesoscopic CsV_3Sb_5 superconducting ring devices, which suggests the possibility of higher-charge superconductivity. Our experimental findings bring new insights into the rich and fascinating quantum states in the kagome superconductors and provide ground work for exploring the physical properties of unprecedented phases of matter formed by multi-particle bound states.

References and Notes

1. J. R. Schrieffer, Theory of superconductivity Perseus Books. *Reading* (1999).
2. J. Bardeen, L. N. Cooper, J. R. Schrieffer, Theory of superconductivity. *Phys. Rev.* **108**, 1175 (1957).
3. B. S. Deaver, W. M. Fairbank, Experimental evidence for quantized flux in superconducting cylinders. *Phys. Rev. Lett.* **7**, 43–46 (1961).
4. R. Doll, M. Näbauer, Experimental proof of magnetic flux quantization in a superconducting ring. *Phys. Rev. Lett.* **7**, 51 (1961).
5. N. Byers, C. N. Yang, Theoretical considerations concerning quantized magnetic flux in superconducting cylinders. *Phys. Rev. Lett.* **7**, 46–49 (1961).
6. D. F. Agterberg, H. Tsunetsugu, Dislocations and vortices in pair-density-wave superconductors. *Nat. Phys.* **4**, 639-642 (2008).
7. E. Berg, E. Fradkin, S. A. Kivelson, Charge- $4e$ superconductivity from pair-density-wave order in certain high-temperature superconductors. *Nat. Phys.* **5**, 830-833 (2009).
8. L. Radzihovsky, A. Vishwanath, Quantum liquid crystals in an imbalanced Fermi gas: fluctuations and fractional vortices in Larkin-Ovchinnikov states. *Phys. Rev. Lett.* **103**, 010404 (2009).
9. D. F. Agterberg, M. Geracie, H. Tsunetsugu, Conventional and charge-six superfluids from melting hexagonal Fulde-Ferrell-Larkin-Ovchinnikov phases in two dimensions. *Phys. Rev. B* **84**, 014513 (2011).
10. S. Jian, Y. Huang, H. Yao, Charge- $4e$ superconductivity from nematic superconductors in two and three dimensions. *Phys. Rev. Lett.* **127**, 227001 (2021).
11. R. M. Fernandes, L. Fu, Charge- $4e$ superconductivity from multi-component nematic pairing: Application to twisted bilayer graphene. *Phys. Rev. Lett.* **127**, 047001 (2021).
12. S. Zhou, Z. Wang, Chern Fermi pocket, topological pair density wave, and charge- $4e$ and charge- $6e$ superconductivity in kagome superconductors, *Nat. Commun.* **13**, 7288 (2022).
13. E. Fradkin, S. A. Kivelson, J. M. Tranquada, Colloquium: Theory of intertwined orders in high temperature superconductors. *Rev. Mod. Phys.* **87**, 457 (2015).
14. D. F. Agterberg *et al.*, The physics of pair-density waves: cuprate superconductors and beyond. *Annu. Rev. Condens. Matter Phys.* **11**, 231 (2020).
15. R. M. Fernandes, P. P. Orth, J. Schmalian, Intertwined vestigial order in quantum materials: Nematicity and beyond. *Annu. Rev. Condens. Matter Phys.* **10**, 133-154 (2019).
16. B. R. Ortiz *et al.*, New kagome prototype materials: discovery of KV_3Sb_5 , RbV_3Sb_5 , and CsV_3Sb_5 . *Phys. Rev. Mater.* **3**, 094407 (2019).
17. B. R. Ortiz *et al.*, CsV_3Sb_5 : A Z_2 topological kagome metal with a

- superconducting ground state. *Phys. Rev. Lett.* **125**, 247002 (2020).
- 18.C. Zhao *et al.*, Nodal superconductivity and superconducting domes in the topological kagome metal CsV₃Sb₅. *arXiv:2102.08356* (2021).
 - 19.H. Zhao *et al.*, Cascade of correlated electron states in a kagome superconductor CsV₃Sb₅. *Nature* **599**, 216–221 (2021).
 - 20.F. Yu *et al.*, Concurrence of anomalous Hall effect and charge density wave in a superconducting topological kagome metal. *Phys. Rev. B* **104**, 041103 (2021).
 - 21.H. Tan *et al.*, Charge density waves and electronic properties of superconducting kagome metals. *Phys. Rev. Lett.* **127**, 046401 (2021).
 - 22.H. Chen *et al.*, Roton pair density wave in a strong-coupling kagome superconductor. *Nature* **599**, 222-228 (2021).
 - 23.Y. Jiang *et al.*, Unconventional chiral charge order in kagome superconductor KV₃Sb₅. *Nat. Mater.* **20**, 1353–1357 (2021).
 - 24.Z. Liang *et al.*, Three-dimensional charge density wave and surface-dependent vortex-core states in a kagome superconductor CsV₃Sb₅. *Phys. Rev. X* **11**, 031026 (2021).
 - 25.S. Yang *et al.*, Giant, unconventional anomalous Hall effect in the metallic frustrated magnet candidate, KV₃Sb₅. *Sci. Adv.* **6**, eabb6003 (2020).
 - 26.H. Xu *et al.*, Multiband superconductivity with sign-preserving order parameter in kagome superconductor CsV₃Sb₅. *Phys. Rev. Lett.* **127**, 187004 (2021).
 - 27.K. Chen *et al.*, Double superconducting dome and triple enhancement of T_c in the kagome superconductor CsV₃Sb₅ under high pressure. *Phys. Rev. Lett.* **126**, 247001 (2021).
 - 28.Y. Xiang *et al.*, Two-fold symmetry of c-axis resistivity in topological kagome superconductor CsV₃Sb₅ with in-plane rotating magnetic field. *Nat. Commun.* **12**, 6727 (2021).
 - 29.III. C. Mielke *et al.*, Time-reversal symmetry-breaking charge order in a kagome superconductor. *Nature* **602**, 245–250 (2022).
 - 30.L. Yu *et al.*, Evidence of a hidden flux phase in the topological kagome metal CsV₃Sb₅. *arXiv:2107.10714* (2021).
 - 31.W. Duan *et al.*, Nodeless superconductivity in the kagome metal CsV₃Sb₅. *Sci. China Phys. Mech. Astron.* **64**, 107462 (2021).
 - 32.W. A. Little, R. D. Parks, Observation of quantum periodicity in the transition temperature of a superconducting cylinder. *Phys. Rev. Lett.* **9**, 9 (1962).
 - 33.V. G. Kogan, J. R. Clem, R. G. Mints, Properties of mesoscopic superconducting thin-film rings: London approach. *Phys. Rev. B* **69**, 064516 (2004).
 - 34.J. H. Han, A. Lee Patrick, Understanding resistance oscillation in CsV₃Sb₅ superconductor. *Phys. Rev. B* **106**, 184515 (2022).
 - 35.V. B. Geshkenbein, A. I. Larkin, A. Barone, Vortices with half magnetic flux quanta in “heavy-fermion” superconductors. *Phys. Rev. B* **36**, 235 (1987).

- 36.H.-Y. Kee, Y. B. Kim, K. Maki, Half-quantum vortex and d-soliton in Sr₂RuO₄. *Phys. Rev. B* **62**, R9275 (2000).
- 37.M. Sigrist, T. M. Rice, K. Ueda, Low-field magnetic response of complex superconductors. *Phys. Rev. Lett.* **63**, 1727 (1989).
- 38.M. A. Rampp, J. Schmalian, Integer and fractionalized vortex lattices and off-diagonal long-range order. *J. Phys. Commun.* **6**, 055013 (2022).

Acknowledgments: A portion of this work was carried out at the Synergetic Extreme Condition User Facility (SECUF). We acknowledge discussions with Li Lu, Yanzhao Liu, Yi Liu, Yanan Li, Haoran Ji and Jingchao Fang, and technical assistance from Jiawei Luo, Pengfei Zhan, Chunsheng Gong, Zhijun Tu, Yinbo Ma, and Gaoxing Ma.

Funding: This work was financially supported by the National Natural Science Foundation of China (Grant No. 11888101), the National Key Research and Development Program of China (Grant No. 2018YFA0305604, No. 2018YFE0202600), the National Natural Science Foundation of China (Grant No. 11974430), Beijing Natural Science Foundation (Z180010, Z200005), the Innovation Program for Quantum Science and Technology (2021ZD0302403) and the China Postdoctoral Science Foundation (2022M720270). Z.Q.W. acknowledges support from the U.S. Department of Energy, Basic Energy Sciences Grant No. DE-FG02-99ER45747 and the Cottrell SEED Award No. 27856 from Research Corporation for Science Advancement.

Author contributions: J.W. conceived and instructed the research. Under the guidance of J.W., J.G. and P.W. performed the transport measurements with the assistance of A. W. and J.S.. J.G. and P.W. analyzed the data under the guidance of J.W.. Z.W. contributed to the theoretical explanation. Q.Y. and H.L. grew the single crystals. J.G. and Y.X. fabricated the devices. J.G., P.W., Z.W. and J.W. wrote the manuscript with the input from all authors.

Competing interests: Authors declare that they have no competing interests.

Data and materials availability: All data are available in the main text or the supplementary materials.

Supplementary Materials

Materials and Methods

Supplementary Text

Figs. S1 to S12

References (1–12)

Figures

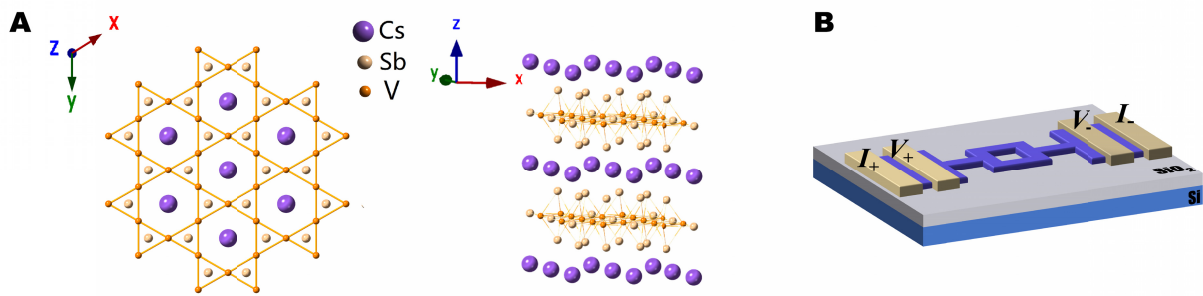


Fig. 1. Schematic crystal structure and drawing of the ring-structure device of CsV₃Sb₅. (A) Schematic crystal structure of CsV₃Sb₅ with purple, orange and yellow spheres denoting Cs, V and Sb atoms, respectively. (B) Schematic drawing of the ring-structure device in the standard four-terminal configuration. The dimensions are not drawn to scale.

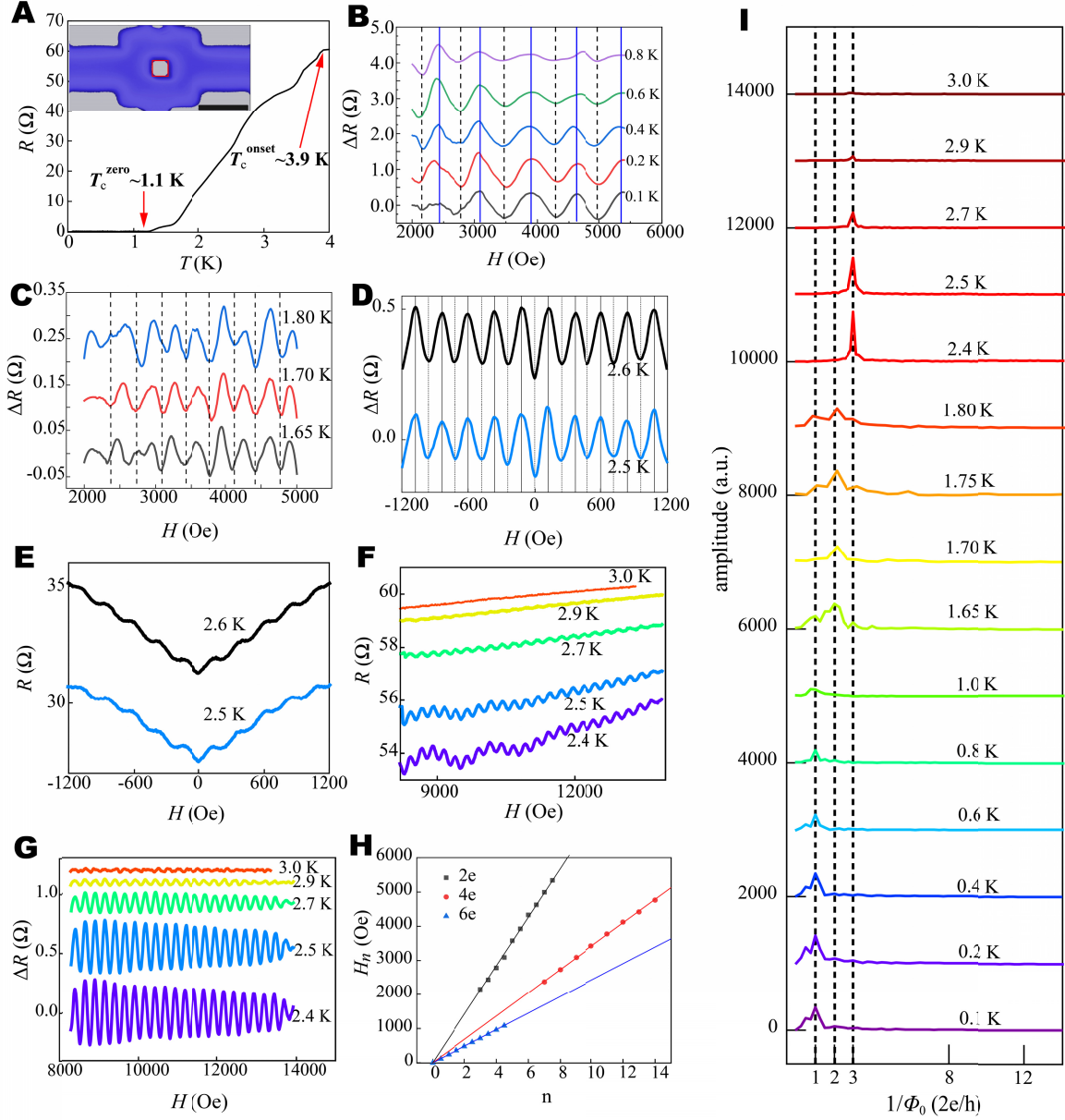


Fig. 2. Evolution of quantum oscillations in superconducting CsV_3Sb_5 ring device s1. (A) Resistance as a function of temperature from 4 K to 0.07 K. Superconductivity with onset temperature ~ 3.9 K and zero-resistance temperature ~ 1.1 K is observed. Inset shows the false-colored image of the CsV_3Sb_5 ring device s1. The sample protected by PMMA layer is represented by blue and the substrate is represented by gray. The scale bar in the false-colored image represents 500 nm. The inner area, middle area and outer area of the ring estimated from the false-colored image is $\sim 0.027 \mu\text{m}^2$, $\sim 0.21 \mu\text{m}^2$ and $\sim 0.54 \mu\text{m}^2$, respectively. (B) $h/2e$ oscillations with period of ~ 750 Oe (the period is obtained from the FFT results in I) in which the rising backgrounds have been subtracted as a function of

the perpendicular magnetic field. The black dashed lines and the blue solid lines label the dips and peaks of the oscillations, respectively. For clarity, data curves are shifted. The effective area of the $h/2e$ oscillations ($\sim 0.0276 \mu\text{m}^2$) is marked by the red rectangle in the inset of (A). (C) Oscillations with period of ~ 350 Oe (the period is obtained from the FFT results in I) at higher temperatures after subtracting smooth backgrounds. The dashed lines label the oscillation dips. For clarity, data curves are shifted. The period of the oscillations (~ 350 Oe) is nearly $1/2$ of that of the $h/2e$ oscillations (~ 750 Oe). If we consider the effective area of the oscillations with period of ~ 350 Oe is the same as that of the $h/2e$ oscillations with period of ~ 750 Oe, then the period of ~ 350 Oe will correspond to a periodicity of $h/4e$. (D) Oscillations with period of ~ 250 Oe at still higher temperatures. For clarity, data curves are shifted. The black dashed and solid lines label the dips and peaks of the oscillations, respectively. The period of the oscillations (~ 250 Oe) is $1/3$ of that of the $h/2e$ oscillations (~ 750 Oe). If we consider the effective area of the oscillations with period of ~ 250 Oe is the same as that of the $h/2e$ oscillations with period of ~ 750 Oe, then the period of ~ 250 Oe will correspond to a periodicity of $h/6e$. (E) Oscillations with period of ~ 250 Oe in the low field region. (F), (G) Oscillations with period of ~ 250 Oe in the high field region. (H) $n-H_n$ index plots of the $h/2e$, $h/4e$ and $h/6e$ oscillations. Here, n is an integer or half integer. Integer n represents the oscillation dip and half integer n represents the oscillation peak. The linear relation between n and H_n can be clearly observed, indicating that the $h/2e$, $h/4e$ and $h/6e$ oscillations are periodic. (I) FFT results as a function of inverse magnetic flux in unit of $2e/h$ at various temperatures. With increasing temperature, the changes in periodicity from $h/2e$ to $h/4e$ and then to $h/6e$ can be clearly observed.

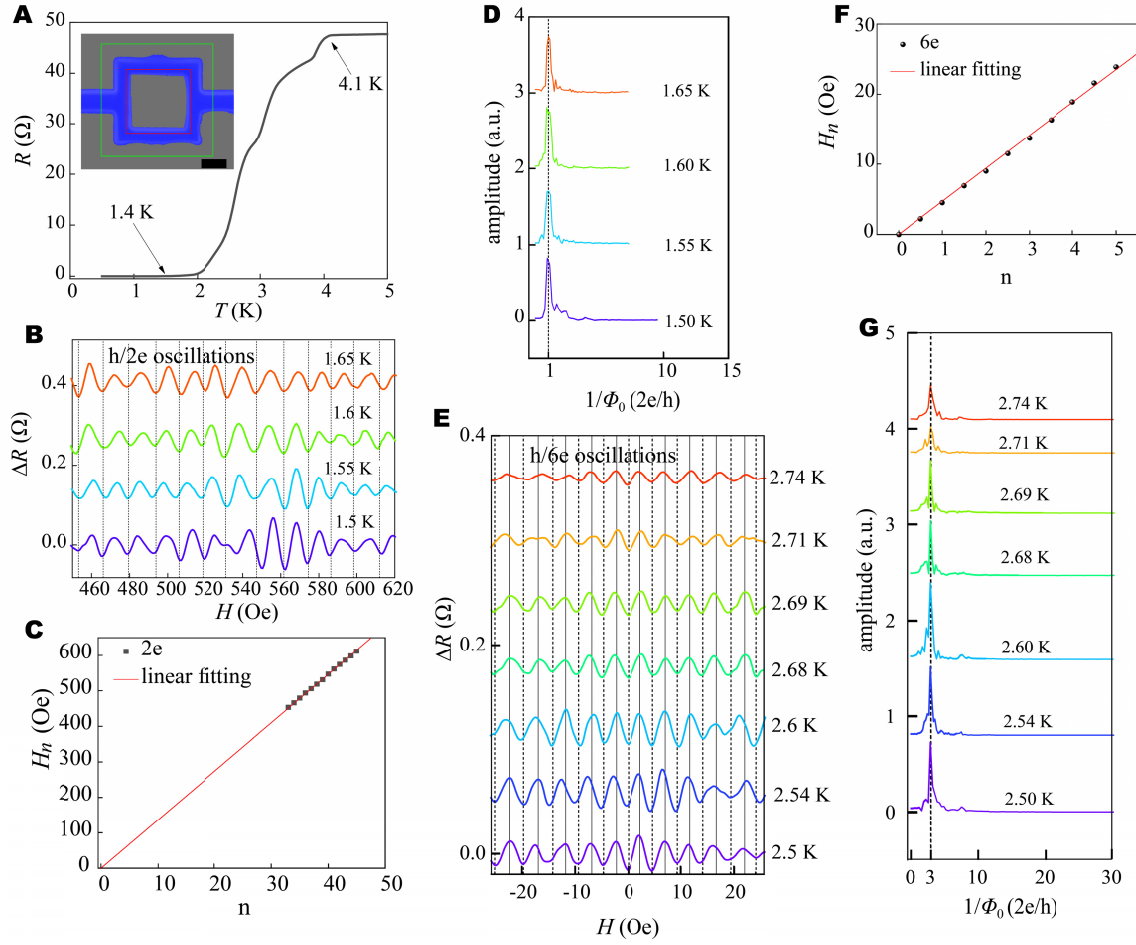


Fig. 3. $h/2e$ and $h/6e$ oscillations in the superconducting CsV_3Sb_5 ring device s2. (A) Resistance as a function of temperature from 5 K to 0.5 K. Superconductivity with onset temperature ~ 4.1 K and zero-resistance temperature ~ 1.4 K is observed. Inset shows the false-colored image of the CsV_3Sb_5 ring device s2. The sample protected by PMMA layer is represented by blue and the substrate is represented by gray. The scale bar in the false-colored image represents 500 nm. The inner area, middle area and outer area of the ring estimated from the false-colored image is $\sim 0.96 \mu\text{m}^2$, $\sim 2.01 \mu\text{m}^2$ and $\sim 2.97 \mu\text{m}^2$, respectively. (B) $h/2e$ oscillations with period of ~ 13.6 Oe (the period is obtained from the FFT results in D) after subtracting smooth backgrounds. The dashed lines label the oscillation dips. For clarity, data curves are shifted. The effective area of the $h/2e$ oscillations ($\sim 1.52 \mu\text{m}^2$) is marked by the red rectangle in the inset of (A). (C) n - H_n index plot of the $h/2e$ oscillations. Here, n is an integer, representing the oscillation dip. A linear relation between n and H_n can be clearly observed, indicating that the magnetoresistance oscillations are periodic. (D) FFT results of the $h/2e$ oscillations. (E) Oscillations with period of ~ 4.6 Oe (the period is obtained from the FFT

results in G) after subtracting smooth backgrounds. The dashed and solid lines label the oscillation dips and peaks, respectively. For clarity, data curves are shifted. The period of the oscillations (4.6 Oe) is nearly 1/3 of that of the $h/2e$ oscillations (13.6 Oe). If the oscillations with period of ~ 4.6 Oe were $h/2e$ oscillations, the effective area ($\sim 4.5 \mu\text{m}^2$, shown by the green rectangle in the inset of (A)) would be obviously much larger than the outer area of the ring device ($\sim 2.97 \mu\text{m}^2$), which is physically impossible. If we consider the effective area of the oscillations with period of ~ 4.6 Oe is the same as that of the $h/2e$ oscillations with period of ~ 13.6 Oe, then the period of ~ 4.6 Oe will correspond to a periodicity of $h/6e$. (F) n - H_n index plot of the $h/6e$ oscillations. Here, n is an integer or half integer, representing the oscillation dip and peak, respectively. The linear relation between n and H_n confirms that the magnetoresistance oscillations are periodic. (G) FFT results of the $h/6e$ oscillations.

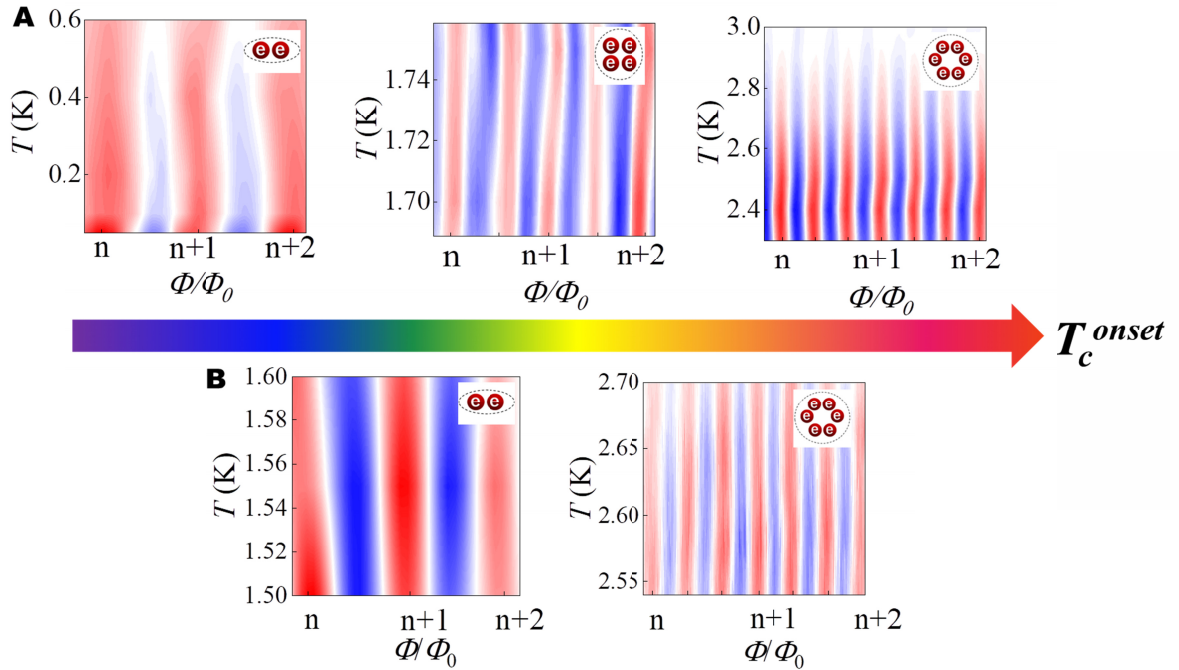


Fig. 4. Phase diagram of the $h/2e$, $h/4e$ and $h/6e$ flux quantization in CsV_3Sb_5 ring device s1 (inner area $\sim 0.027 \mu\text{m}^2$) (A), and $h/2e$ and $h/6e$ flux quantization in CsV_3Sb_5 ring device s2 (inner area $\sim 0.96 \mu\text{m}^2$) (B). Charge- $2e$, $4e$ and $6e$ flux quantization are identified by the periodicity of the corresponding magnetoresistance oscillations. The oscillations are presented as intensity maps of ΔR on the temperature T and magnetic flux Φ/Φ_0 plane. With increasing temperature (T), the periodicity changes from $h/2e$ to $h/4e$ and then to $h/6e$ in smaller ring device s1. In larger ring structure s2, the periodicity changes from $h/2e$ to $h/6e$.